Delft University of Technology

The developing flow profile of the suspension in a Semi-Solid Flow Battery

Author:
Kyle Muller

Supervisor and first examiner:
Dr. Martin Rohde

Second examiner:
Dr. Erik Kelder

TU Delft
Faculty of Applied Sciences
BSc program Applied Physics
November 30, 2020

Abstract

The development of the flow within a Semi-Solid Flow Battery (SSFB) is analyzed, modelled and used to determine the electrical conductivity of the suspension in the SSFB. The flow is modelled using the Lattice Boltzmann Method, after which data correlating the shear rate and the electrical conductivity of the suspension is used to model the electrical conductivity throughout the SSFB. First a Poiseuille flow is modelled in order to check whether the Lattice Boltzmann method is suitable for the modelling of a developing flow. The results of the modelling of the Poiseuille flow indicate that, due to an erroneously applied boundary condition, the flow development is inaccurately modelled near the inlet of the flow cell. The developed flow away from the inlet is accurate and converges to the analytical solution for a Poiseuille flow, confirming that the Lattice Boltzmann Method is suitable for modelling developing flows. The Lattice Boltzmann Method is then used to model the developing flow of a non-Newtonian suspension. From the electrical conductivity of the non-Newtonian suspension a electronic resistance profile along the length of the flow cell is determined, showing variance of electronic resistance based on position within the flow cell. Using the variance of electronic resistance it can be determined that the electronic resistance in the SSFB is path dependent. It can be concluded from the determined electronic resistance profile and development profile that the development of the flow within a Semi-Solid Flow Battery only significantly affects the electronic resistance near the inlet of the flow cell.

Contents

1 Introduction **1**
1.1 What is a Semi Solid Flow Battery . . . 1
1.2 Problem Description . . . 2
1.3 Research question . . . 2

2 Theory **3**
2.1 The carbon additive of the suspension in the Semi-Solid Flow Battery . . . 3
2.2 Rheology of the suspension in the Semi-Solid Flow Battery . . . 5
2.3 Modelling the velocity profile . . . 6
2.3.1 Navier-Stokes model . . . 6
2.3.2 Lattice Boltzmann Method . . . 6

3 Method **8**
3.1 Modelling a Poiseuille flow . . . 8
3.1.1 Initial conditions . . . 8
3.1.2 Boundary conditions . . . 9
3.2 Modeling a non-Newtonian flow . . . 12
3.3 Determining the electrical conductivity profile . . . 15

4 Results **16**
4.1 Poiseuille Flow . . . 16
4.1.1 Stability of the flow profile . . . 16
4.1.2 Development of the flow profile . . . 17
4.2 Modeling a non-Newtonian flow . . . 20
4.3 Determining the electrical conductivity profile . . . 24

5 Discussion **27**
5.1 Development of the flow . . . 27
5.2 Shear rate and electrical conductivity profiles . . . 27

6 Conclusion **28**

7 Recommendations **29**

Bibliography **30**

1 Introduction

In today's climate, with the dwindling of resources such as oil, coal, and natural gas, the transition to sustainable energy sources is becoming increasingly important. In order to facilitate this switch the storage of alternate energy is of importance, as the demand for energy and the moment of production for sustainable energies often do not coincide. The storage of this energy in batteries seems like a logical step, however, regular batteries are not considered an economically feasible solution to this energy storage problem.[2] Redox Flow batteries are considered to be one of the few environmentally friendly, and relatively cheap methods for storing large amounts of energy. [7] Flow batteries allow for large amounts of energy to be stored for use at a later moment. An additional advantage of flow batteries is that the energy can be stored in a separate location from where it has to be used, which allows for areas that are not properly connected to an electrical grid to have access to sustainable energy. An issue with RFB's is that in their current state, they cannot store enough energy for the cost they incur, and therefore improvements on RFB's have to be made. [7] A Semi-Solid Flow Battery, as can be seen in figure 1, is such an improvement on a Redox Flow Battery.

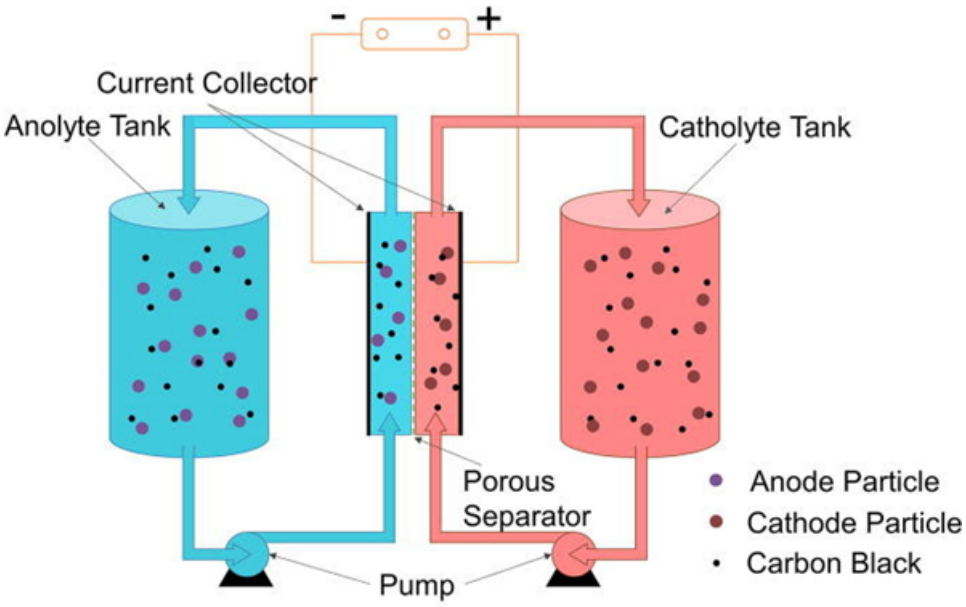

Figure 1: A schematic of a Semi-Solid Flow Battery. [2]

1.1 What is a Semi Solid Flow Battery

A Semi-Solid Flow Battery can be considered a combination between a regular lithium-ion battery and a Redox flow battery. Unlike in a redox flow battery, the anode and cathode of a SSFB are suspensions in which the electroactive materials are suspended in a liquid electrolyte.[2] The suspension allows for significant more energy to be stored in the battery, making them a stark improvement upon the Redox Flow Battery solutions. [6] These suspensions are stored in tanks, and combined with a carbon additive, which allows for electron transport within the suspensions. These tanks can be removed from the battery and transported to other locations, meaning that the battery can be charged in one location, and used in another. The suspensions in the tanks are pumped through a flow cell, where they are separated by a porous separator, through which only Lithium-ions can flow. The current in a semi-solid flow battery is created through redox-reactions. These redox reactions provide the electrons and Li^+ ions required for a current to run through the flow cell. A generic redox-reaction looks as follows [1]:

$$ALi \xrightarrow{charge} ALi_{1-x} + xLi^+ + xe^-(Cathode) \tag{1}$$

$$xLi^+ + xe^- + B \xrightarrow{charge} BLi_x(Anode) \tag{2}$$

When discharging these reactions reverse. The complete redox-reaction looks like

$$ALi + B \xrightarrow{charge} ALi_{1-x} + BLi_x \tag{3}$$

1.2 Problem Description

Since Semi-Solid flow batteries are a relatively new technology,not much is known about them. For this research there are several aspects of the Semi-Solid Flow Battery that are of interest. First, the way the flow profile of the suspension in the flow cell develops will be studied. A developing flow profile implies varying speeds and shear rates, meaning it is important to understand the rheology of the suspension. The electrical conductivity of the suspension in the SSFB is affected by shear rate, therefore the electrical conductivity will be investigated.

1.3 Research question

The research question of this report is: How does the flow profile within the flow cell of a semi-solid flow battery develop, and how does this affect the electrical conductivity?

2 Theory

For this research there are several aspects of the Semi-Solid Flow Battery that are of interest. Firstly, it is important to study the way the flow profile of the suspension in the flow cell develops. Since a developing flow profile implies varying speeds and shear rates which the suspension experiences, it is important to understand the rheology of the suspension. Another aspect to be considered is how the rheology of the suspension affects the electrical conductivity in the SSFB.

2.1 The carbon additive of the suspension in the Semi-Solid Flow Battery

The carbon additive in the Semi-Solid Flow Battery is most commonly Ketjen Black (KB) [4] [5] [6]. This carbon additive is highly effective, as less than 1 $vol\%$ is needed to properly form conducting carbon networks. Besides this the KB also functions as stabilizer, as it prevents the larger electroactive particles in the suspension from separating from the suspension. [6] The KB changes the rheology of any solution it is added to, as with $0.3 - 0.6$ $vol\%$ [6] the solution to which it is added will start showing strong shear thinning behavior, a term explained in section 2.2. Ketjen Black forms conducting carbon networks by forming agglomerates, a combination of several aggregates of KB. The size and electrical conductivity of these formed agglomerates depend on the shear rate that the suspension is experiencing. In figure 2 a relation between shear rate, viscosity and electrical conductivity can be seen.

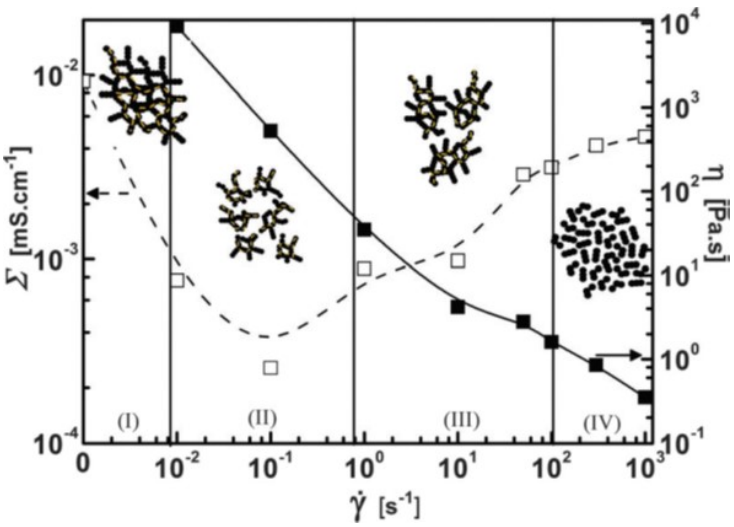

Figure 2: A figure showing the viscosity and electrical conductivity of a solution with 0.021 wt% Ketjen Black as a function of the shear rate the solution experiences. The solid line indicates the viscosity and the dotted line indicates the electrical conductivity.[4]

In figure 2 it can be seen that large, dense carbon networks result in a high viscosity, but also in a high electrical conductivity. This makes sense as these large carbon networks easily connect the electroactive species with the current collector of the SSFB, but their size makes the suspension more viscous. When the shear rate increases, the large carbon networks experience too much force to properly stay together, and they break up into medium sized agglomerates. These medium sized agglomerates give the suspension a lower viscosity, but also a much lower electrical conductivity. Apparently these medium sized agglomerates do not properly connect the electroactive species to the current collector, apparent by them having the lowest overall electrical conductivity. Another increase in shear rate will break up the agglomerates even further, again decreasing the viscosity, but increasing the electrical conductivity of the suspension. This means that small agglomerations of KB have an easier time connecting at higher shear rates and higher speeds. At even higher shear rates the agglomerates break up into individual aggregates, further decreasing the viscosity and increasing the electrical conductivity, as these aggregates seemingly connect very easilly at these shear rates. At smaller size agglomerates the KB particles connect the electroactive species to the current collector by colliding with other KB particles, creating a semblance of a network.

It is apparent that at varying sizes of agglomerates, the electrical conductivity increases and decreases.

- High electrical conductivity - Low or high shear rates - Large agglomerates/Small or individual agglomerates
- Low electrical conductivity - Medium shear rates - Medium agglomerates

This difference in electrical conductivity depending on shear rate means that the flow profile within the Semi-Solid Flow Battery determines the electrical conductivity.

2.2 Rheology of the suspension in the Semi-Solid Flow Battery

The suspension in the Semi-Solid Flow Battery is a non-Newtonian fluid [4], meaning that the viscosity (μ) of the suspension is dependent on the stress the suspension experiences. This means that the suspension of the SSFB does not follow Newtons law for viscosity. Newton's law for viscosity states that:

$$\tau = \mu\dot{\gamma} \tag{4}$$

Here τ is the shear stress and $\dot{\gamma}$ is the shear rate. The shear rate can be defined as [12]:

$$\dot{\gamma} = \frac{\partial u_i}{\partial x_j} + \frac{\partial u_j}{\partial x_i} \tag{5}$$

In equation 5 i and j can take values of the coordinate system, so for Cartesian coordinates they can be x, y and z. For non-Newtonian fluids the viscosity is not considered constant, which means the viscosity (μ) becomes the apparent viscosity (η), which can be a function of the shear rate ($\dot{\gamma}$). For Powerlaw fluids the apparent viscosity can be defined as:

$$\eta(\dot{\gamma}) = k\dot{\gamma}^{n-1} \tag{6}$$

Equation 6 can be used to define the shear stress for Powerlaw fluids as follows

$$\tau = k\dot{\gamma}^{n-1}\dot{\gamma} \tag{7}$$

From equation 7 it becomes apparent that depending on how n is chosen, the shear stress becomes a different function of the shear rate. If $n < 1$, a powerlaw fluid becomes a shear thinning fluid, meaning that the shear stress increases more slowly as the shear rate increases. On the other hand, if $n > 1$, a powerlaw fluid becomes a shear thickening fluid, meaning that the shear stress increases more rapidly as the shear rate increases. Another way that the rheology of a fluid can differ from Newtonian fluids is that a fluid can simply not flow until it experiences a certain shear stress. A fluid like this is known as a Bingham fluid. The way the shear rate effects some of these fluids can be seen in figure 3.

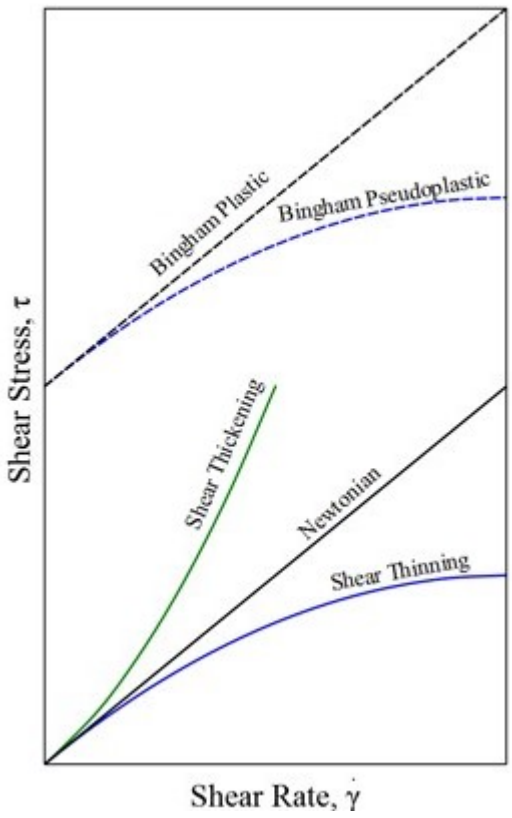

Figure 3: The shear stress plotted as a function of the shear stress for several non-Newtonian fluids, with the bottom left being the origin of the x and y axis.[3]

2.3 Modelling the velocity profile

In order to determine the developing velocity profile of the suspension in the SSFB, a suitable method has to be selected. Initially rewriting the Navier-Stokes equation for a two dimensional cell could provide a solution.

2.3.1 Navier-Stokes model

Starting with the complete Navier-Stokes equation:

$$\frac{\partial \rho v_x}{\partial t} = -\frac{\partial}{\partial x}(v_x \rho v_x) - \frac{\partial}{\partial y}(v_y \rho v_x) - \frac{\partial}{\partial z}(v_z \rho v_x) + \frac{\partial}{\partial x}(\mu \frac{\partial v_x}{\partial x}) + \frac{\partial}{\partial y}(\mu \frac{\partial v_x}{\partial y}) + \frac{\partial}{\partial z}(\mu \frac{\partial v_x}{\partial z}) - \frac{\partial p}{\partial x} + \rho g_x \quad (8)$$

This can be simplified with the conditions that the velocities in the y and z direction are constant, meaning that $\frac{\partial v_y}{\partial x_j} = \frac{\partial v_z}{\partial x_j} = 0$. In addition, the situation is considered steady-state, giving $\frac{\partial \rho v_x}{\partial t} = 0$. This leads to the following equation.

$$0 = -\frac{\partial}{\partial x}(v_x \rho v_x) + \frac{\partial}{\partial x}(\mu \frac{\partial v_x}{\partial x}) + \frac{\partial}{\partial y}(\mu \frac{\partial v_x}{\partial y}) - \frac{\partial p}{\partial x} + \rho g_x \quad (9)$$

This equation could be simplified further, in order to create a discretized Navier-Stokes equation with which a developing velocity profile could be modeled. In order to properly discretize the equation another assumption has to be made, namely $\frac{\partial p}{\partial x}$, the pressure drop, has to be considered as a constant. If this assumption is not made, the equation would contain two variables, making it impossible to solve. The pressure drop however does depend on the change in velocity, and should only be considered constant if the velocity profile is fully developed and unchanging. This means that using the Navier-Stokes equation as a basis for determining the developing velocity profile would result in a systematic error, therefore another method should be considered.

2.3.2 Lattice Boltzmann Method

The Lattice Boltzmann Method is known to be capable of modelling incompressible Navier-Stokes equations, in the limit where density is a constant. [9] The Lattice Boltzmann Method divides the flow cell into many lattice units, within which the particles have have direction vectors. A representation of a lattice unit can be seen in figure 4.

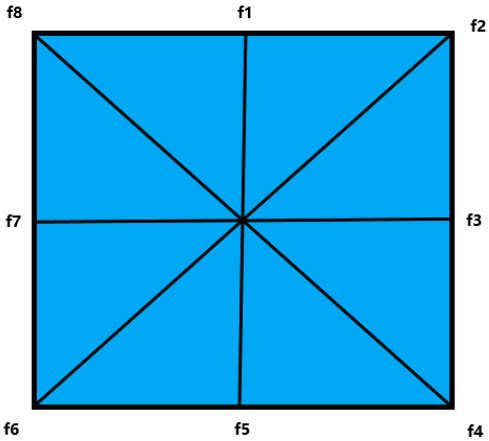

Figure 4: A simplistic representation of the lattice unit and the probability distributions f_k

The vectors denoted as $f_0, f_1, ..., f_8$ describe the distribution functions of the particles moving in the directions $\vec{c}_0, \vec{c}_1, ..., \vec{c}_8$. Since the distribution functions f_k describe all particles within the lattice unit, the density of the particles within the lattice unit can be described as: [8]

$$\Sigma f_k = \rho \tag{10}$$

and the macroscopic flow velocity $\mathbf{u} = (u_x, u_y)$ can be described as: [8]

$$\Sigma f_k \vec{c}_k = \rho \mathbf{u} \tag{11}$$

Since f_k are variables, ρ is also variable, which is not physical behavior. The error caused by this assumption is known as the compressibility error. With $\mathbf{u}$ defined as:

$$\mathbf{u} = \begin{pmatrix} u_x \\ u_y \end{pmatrix} \tag{12}$$

The whole flow cell is described with these lattice units, and they are made to interact with one another. When starting with modeling the flow within the cell, the system only has its boundary conditions defined, and most lattice units experience change between each time step of the model. The equilibrium distribution function f_k^{eq} describes the distribution function when the system reaches its equilibrium. The equilibrium distribution function is defined as [8]:

$$f_k^{eq} = w_k \rho [1 + 3(\vec{c}_k \mathbf{u}) + \frac{9}{2}(\vec{c}_k \mathbf{u})^2 - \frac{3}{2}\mathbf{u} * \mathbf{u}] \tag{13}$$

Here w_k and c_k are respectively the weights and direction vectors of the particle distributions, which are defined by Zou and He [8] as:

$$w_0 = \frac{4}{9}, w_1 = w_3 = w_5 = w_7 = \frac{1}{9}, w_2 = w_4 = w_6 = w_8 = \frac{1}{36}$$

The sum of these weights is one, which allows for the particle distributions to be defined as $f_k = w_k * \rho$. The directions of the particle distributions $\vec{c}_0, \vec{c}_1, ..., \vec{c}_8$ are defined as:

$$\vec{c}_0 = \begin{pmatrix} 0 \\ 0 \end{pmatrix}, \vec{c}_1 = \begin{pmatrix} 0 \\ 1 \end{pmatrix}, \vec{c}_2 = \begin{pmatrix} 1 \\ 1 \end{pmatrix}, \vec{c}_3 = \begin{pmatrix} 1 \\ 0 \end{pmatrix}, \vec{c}_4 = \begin{pmatrix} 1 \\ -1 \end{pmatrix},$$

$$\vec{c}_5 = \begin{pmatrix} 0 \\ -1 \end{pmatrix}, \vec{c}_6 = \begin{pmatrix} -1 \\ -1 \end{pmatrix}, \vec{c}_7 = \begin{pmatrix} -1 \\ 0 \end{pmatrix}, \vec{c}_8 = \begin{pmatrix} -1 \\ 1 \end{pmatrix}$$

The distribution function f_k can be related to f_k^{eq} by the Bhatnagar-Gross-Krook approximation [11], which looks as follows.

$$f_k(\mathbf{x} + c_k \Delta x, t + \Delta t) = f_k(\mathbf{x}, t) - \frac{f_k(\mathbf{x}, t) - f_k^{eq}(\mathbf{x}, t)}{\tau} \tag{14}$$

The fraction in equation 14 is known as the collision operator of the Lattice Boltzmann Method. Here τ is the relaxation time, which controls how long it takes to reach the equilibrium state. This relaxation time is a function of the apparent viscosity ν. Another way the lattice units interact with one another is through streaming, meaning that particle distributions move in the direction in which they point. This means that $f_k(x, t) = f_k(x + c_k \Delta t, t + \Delta t)$. To more clearly explain this an example will be shown of how distribution function f_2 moves after 1 time step. At time t there is a distribution function f_2 at location $x = i$ and $y = j$. This distribution then streams, taking a time of dt. Since f_2 has a direction of $\vec{c}_2 = [1, 1]$, the streaming process looks as follows:

$$f_2^t(i, j) = f_2^{t+dt}(i + 1, j + 1) \tag{15}$$

The collision and the streaming step describe how the lattice units interact with one another, and iterating these steps provides a model of a developing stream in the flow cell. The boundary conditions of this model will be discussed in section 3.1.

3 Method

3.1 Modelling a Poiseuille flow

In order to check whether the Lattice Boltzman Method can properly model a flow profile of the suspension in the SSFB, first a basic Poiseuille flow is modeled. This means that the suspension is considered to be a Newtonian fluid.

In order to start building the model, first a process has to be established for how the model will function. The first step in setting up the model is initializing the lattice and the particle distributions along with determining what the boundary conditions of the system are.

3.1.1 Initial conditions

First, the flow cell and its contents have to be defined. In figure 5 the initial conditions and constants within the flow cell can be seen.

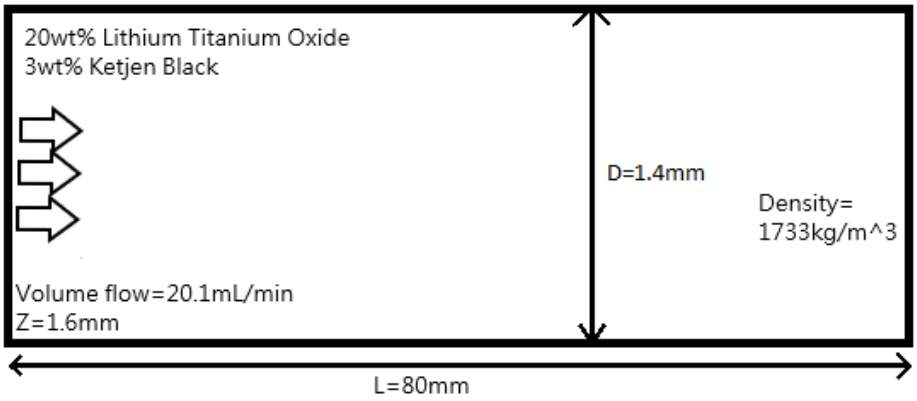

Figure 5: Schematic representation of the flow cell and the initial conditions

The schematic in figure 5 describes the experimental set-up of the Semi Solid Flow Battery used by Duduta et al [6] and a suspension with 20 wt% Lithium Titanium Oxide ($Li_4Ti_5O_{12}$, (LTO)) and 3 wt% of Ketjen Black used by Madec et al [5]. The suspension flows in the x-direction, along the length of the flow cell with a volumetric flow of $20.1mL/min$. From this flow rate and the dimensions of the flow cell, the initial velocity can be determined, leading to a flow speed of $u_x = 0.15m/s$ at the inlet of the flow cell. Since the chosen solution is a non-Newtonian fluid, it does not have a constant apparent viscosity. In order to model a Poiseuille flow, an apparent viscosity can simply be chosen. For this model the lowest possible apparent viscosity of $Li_4Ti_5O_{12}$ is chosen from figure 7, meaning that $\nu_{real} = 1.04e-5Pa/s$. The reason the lowest possible ν is chosen is because this gives the most stable model. [11]

Since the entire model needs to be expressed in Lattice Boltzmann units, a lattice has to be created. This is simply done by defining the width and height of the flow cell in integers. For this particular model they were defined as follows: $widthsize = 40lbu$ and $lengthsize = 75lbu$. These sizes are selected to create a resolution in the model that allows for the changing flow to be properly studied, whilst allowing for the flow profile to be calculated relatively quickly. The width of the flow cell is fully defined, however only the start of length is checked. This is done because in order to check the full length of the flow cell, the length size would have to be defined as $lengthsize = widthsize\frac{L}{D} \approx 2285$, which requires too much computing power. Having defined the lattice, the flow cell still needs to be filled, as lattice units with no particle distributions f_k are considered empty. In order to fill up the lattice, equation 10 is used, and the density of the fluid is defined as the density at the outlet. The particle distributions are defined as $f_k = w_k * \rho$, using the weights from section 2.3.2.

Having defined ν in real units, it has to be defined in Lattice Boltzmann units. The lowest possible ν for which the model is stable in Lattice Boltzmann units is $\nu_{lbm} = 0.001$ [11], however, in order to ensure the stability of the model, the lowest value of ν possible is set to $\nu_{lbm} = 0.033$.

Now only the initial velocity of the suspension has to be rewritten into Lattice Boltzmann units. In order to properly do this, the Reynolds number is set to be equivalent between the real system and the Lattice Boltzmann model. [13]

$$Re_{real} = Re_{lbm} \tag{16}$$

$$\frac{u_{x,real} D_{real}}{\nu_{real}} = \frac{u_{x,lbm} D_{lbm}}{\nu_{lbm}} \tag{17}$$

Knowing all but one variable from equation 17, $u_{x,lbm}$ can be determined.

$$u_{x,lbm} = \frac{u_{x,real} D_{real}}{\nu_{real}} \frac{\nu_{lbm}}{D_{lbm}} = 0.017[lbu/lt] \tag{18}$$

With all constants known in Lattice Boltzmann units, and a filled lattice, the model can be properly initiated.

3.1.2 Boundary conditions

All needed parameters to model the flow have been determined. As described in section 2.3.2, in order to perform the collision step in the model, the equilibrium particle distributions have the be known. The equilibrium particle distribution as defined in equation 13 can be determined with the known parameters, so the collision step can be determined. The collision step as defined in equation 14 is rewritten in order to determine the particle distribution after a time step. The particle distribution after the collision step looks as follows:

$$f^{t^*}_{i,j,k} = f^t_{i,j,k} - \frac{1}{\tau^t_{i,j}} [f^t_{i,j,k} - f^{eq,t}_{i,j,k}] \tag{19}$$

All particle distributions in this equation are known, and therefore the collision step can be calculated. The streaming step described in equation 15 can be defined for all $f^{t+1}_{i,j,k}$

$$\begin{pmatrix} f_{i,j,0} \\ f_{i,j+1,1} \\ f_{i+1,j+1,2} \\ f_{i+1,j,3} \\ f_{i+1,j-1,4} \\ f_{i,j-1,5} \\ f_{i-1,j-1,6} \\ f_{i-1,j,7} \\ f_{i-1,j+1,8} \end{pmatrix}^{t+1} = \begin{pmatrix} f_{i,j,0} \\ f_{i,j,1} \\ f_{i,j,2} \\ f_{i,j,3} \\ f_{i,j,4} \\ f_{i,j,5} \\ f_{i,j,6} \\ f_{i,j,7} \\ f_{i,j,8} \end{pmatrix}^{t^*} \tag{20}$$

Now it should be noted that after the streaming step, certain particle distributions have to be defined. After streaming, at the top flow cell wall, particle distributions f_1, f_2 and f_8 are undefined, meaning that they have to be defined differently. Using equations 10 and 11, the density and the particle distributions f_1, f_2 and f_8 can be defined as:

$$\rho = \frac{1}{1 - u_y} [f_0 + f_3 + f_7 + 2(f_4 + f_5 + f_6)] \tag{21}$$

$$f_1 = f_5 + \frac{2}{3} \rho u_y \tag{22}$$

$$f_2 = f_6 - \frac{1}{2}(f_3 - f_7) + \frac{1}{2} \rho u_x + \frac{1}{6} \rho u_y \tag{23}$$

$$f_8 = f_4 + \frac{1}{2}(f_3 - f_7) - \frac{1}{2} \rho u_x + \frac{1}{6} \rho u_y \tag{24}$$

The derivations of these equations can be found in papers by Zou & He [8] or Alankar et al [10]. At the bottom wall the equations for the unknown particle distributions can be found by rewriting equations 22, 23 and 24. Since the no slip condition exists on the walls of the flow cell, equations 22, 23 and 24 simplify, as $u_x = u_y = 0$.

At the inlet of the flow cell ρ, f_2, f_3 and f_4 are unknown. Once again, using equations 10 and 11 these unknown values can be defined by the known values.

$$\rho_{inlet} = \frac{1}{1 - u_{x,inlet}}[f_0 + f_1 + f_5 + 2(f_6 + f_7 + f_8)] \tag{25}$$

$$f_3 = f_7 + \frac{2}{3}\rho_{in}u_x \tag{26}$$

$$f_2 = f_6 - \frac{1}{2}(f_3 - f_7) + \frac{1}{6}\rho u_x \tag{27}$$

$$f_4 = f_8 + \frac{1}{2}(f_3 - f_7) + \frac{1}{6}\rho u_x \tag{28}$$

In order to define the unknown particle distributions at the outlet (f_6, f_7 and f_8), first the velocity at the outlet needs to be defined. The density ρ_{out} at the outlet is known, allowing for the velocity u_x to be defined as:

$$u_{x,outlet} = 1 - \frac{f_0 + f_1 + f_5 + 2(f_2 + f_3 + f_4)}{\rho_{out}} \tag{29}$$

Particle distributions f_6, f_7 and f_8 can be obtained from equations 26, 27 and 28, by rewriting ρ_{inlet} as ρ_{outlet} and $u_{x,inlet}$ as $u_{x,outlet}$.

The only point left that has undefined values after the streaming step are the corner points of the flow cell. Take the bottom node at the inlet for example, here only f_5, f_6 and f_7 are known. A bounce-back condition makes it so that we can define $f_1 = f_5$, $f_3 = f_7$ and $f_2 = f_6$. The remaining particle distributions can be defined as $f_4 = f_8 = \frac{1}{2}[\rho - (f_0 + f_1 + f_2 + f_3 + f_5 + f_6 + f_7)]$. The only problem with this final definition is that ρ is not defined at the inlet corner nodes, therefore the density is taken to be equal to the density of the adjacent lattice unit in the inlet. At the outlet corner nodes the unknown values can be determined in a similar way. With all boundaries and initial values properly defined, the process by which the model for a developing flow is made can be determined. The process can be seen in figure 6. [10]

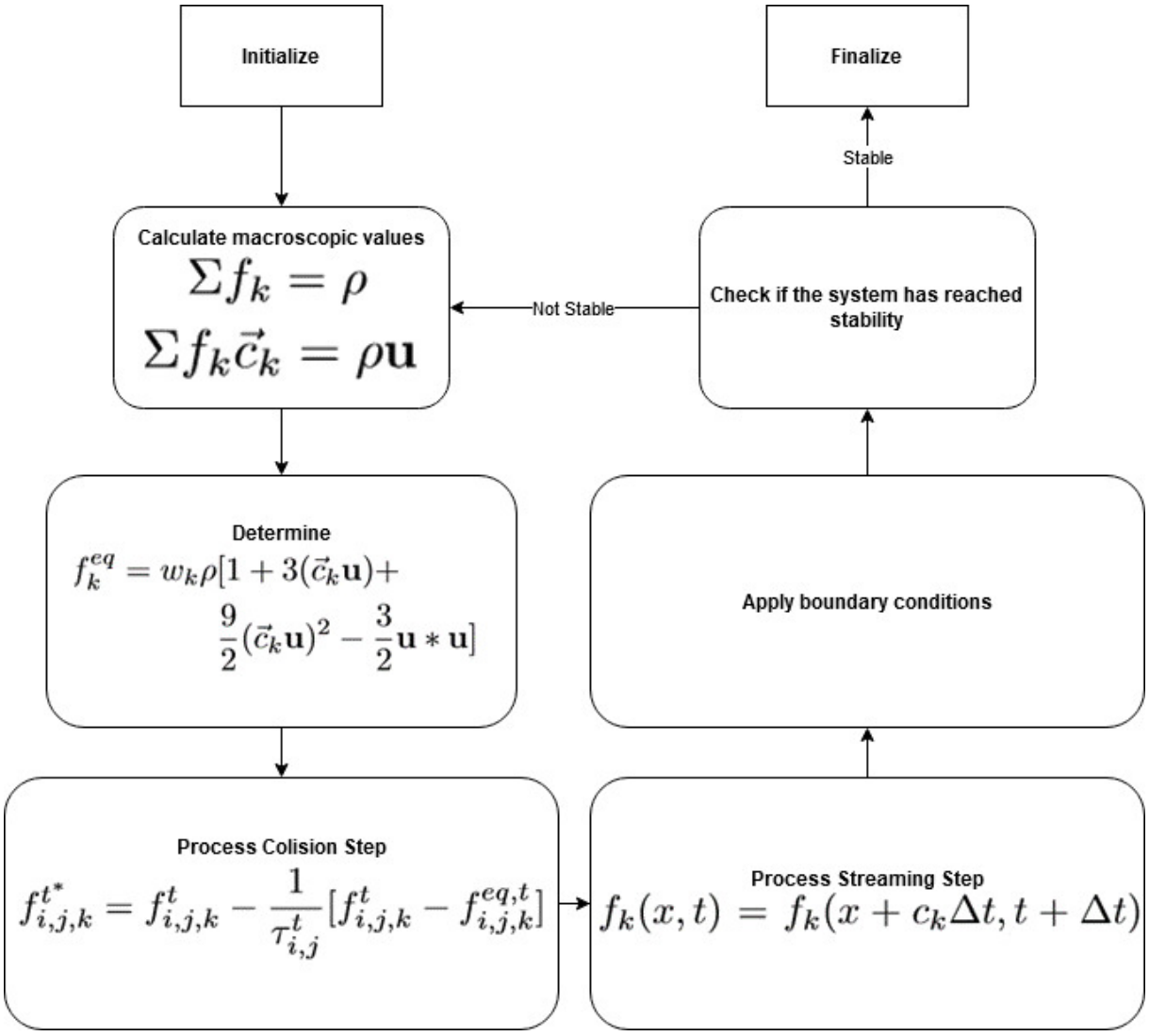

Figure 6: Flowchart showing the process of modelling a Poiseuille flow

3.2 Modeling a non-Newtonian flow

In order to model a non-Newtonian fluid, the model described in section 3.1 has to be altered. A non-Newtonian fluid has a viscosity that is a function of the shear rate, namely $\eta(\dot{\gamma})$. Within the model described in section 3.1 the only variable that changes is τ since this is dependent on ν. The apparent viscosity ν has now becomes a function of the shear rate, since $\nu = \eta(\dot{\gamma})/\rho$. The shear rate in 2D can be defined as [12]:

$$\dot{\gamma} = \sqrt{\frac{1}{2}\dot{\gamma}_{ij}\dot{\gamma}_{ji}} \tag{30}$$

Here $\dot{\gamma}_{ij}$ is defined as:

$$\dot{\gamma}_{ij} = \frac{\partial u_i}{\partial j} + \frac{\partial u_j}{\partial i} \tag{31}$$

In equation 31 the subscripts i and j denote the coordinates x and y, meaning that i and j take the value of both of these coordinates. Since $u_y = 0$ everywhere in the the flow cell, for the model, can be simplified to [12]:

$$\dot{\gamma} = \sqrt{2\frac{\partial u_x}{\partial x}^2 + \frac{\partial u_x}{\partial y}^2} \tag{32}$$

Now equation 32 has to be discretized, since the change in velocity can only be expressed as a difference between the velocity of two points in the lattice, and cannot be defined as a continuous function. In order to discretize the derivative of the velocity u_x, the central difference method [15] is used.

$$\frac{\partial u_x}{\partial x} = \frac{u_{x,i+1,j} - u_{x,i-1,j}}{2\Delta x} \tag{33}$$

$$\frac{\partial u_x}{\partial y} = \frac{u_{x,i,j+1} - u_{x,i,j-1}}{2\Delta y} \tag{34}$$

For points at the top wall and inlet the forward difference method in equation 35 is used.[15]

$$\frac{\partial u_x}{\partial x} = \frac{u_{x,i+1,j} - u_{x,i,j}}{\Delta x} \tag{35}$$

For points at the bottom wall and outlet the backward difference method in equation 36 is used.[15]

$$\frac{\partial u_x}{\partial x} = \frac{u_{x,i,j} - u_{x,i-1,j}}{\Delta x} \tag{36}$$

For $\frac{\partial u_x}{\partial y}$ a similar procedure can be done. It has to be noted that $\Delta x = \Delta y = 1$ since x and y are defined in Lattice Boltzmann units.

Now that the shear rate can be determined from the model, the viscosity can be determined from the relation between the shear rate and the viscosity in figure 7.

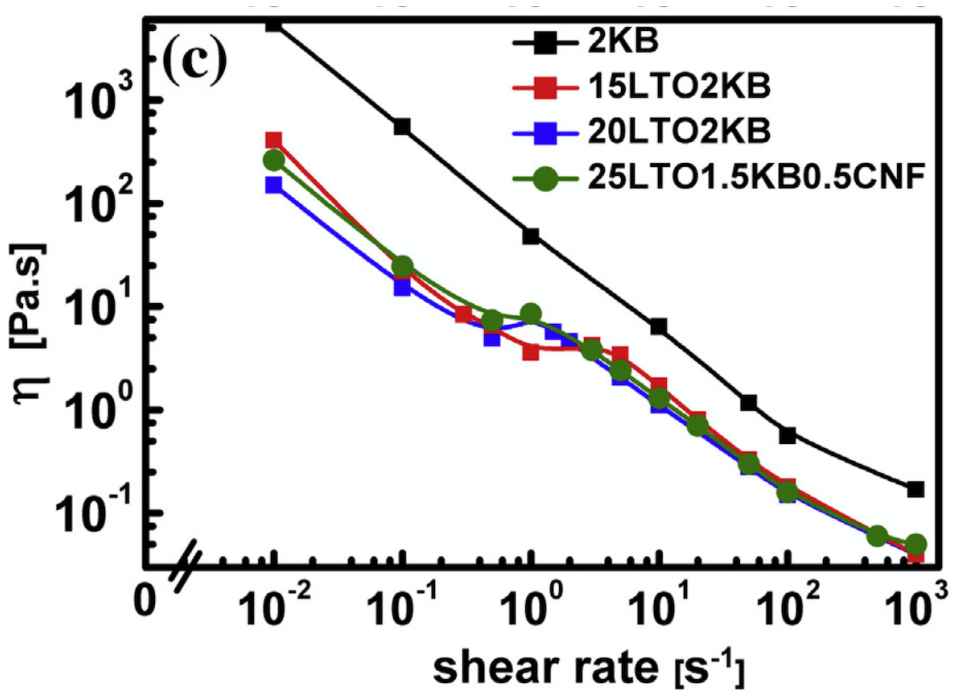

Figure 7: Data correlating the viscosity η to the shear rate $\dot{\gamma}$ [5].

The data for the suspension 20LTO2KB from figure 7 is extrapolated using WebPlotDigitizer [14].

Now that the viscosity can be determined from the model, the relaxation time τ can be calculated via $\tau = (6\nu + 1)/2$. This new relaxation time is then used in calculating the collision step via equation 19. The process to model a developing flow described in figure 6 is adapted into the process shown in figure 8.

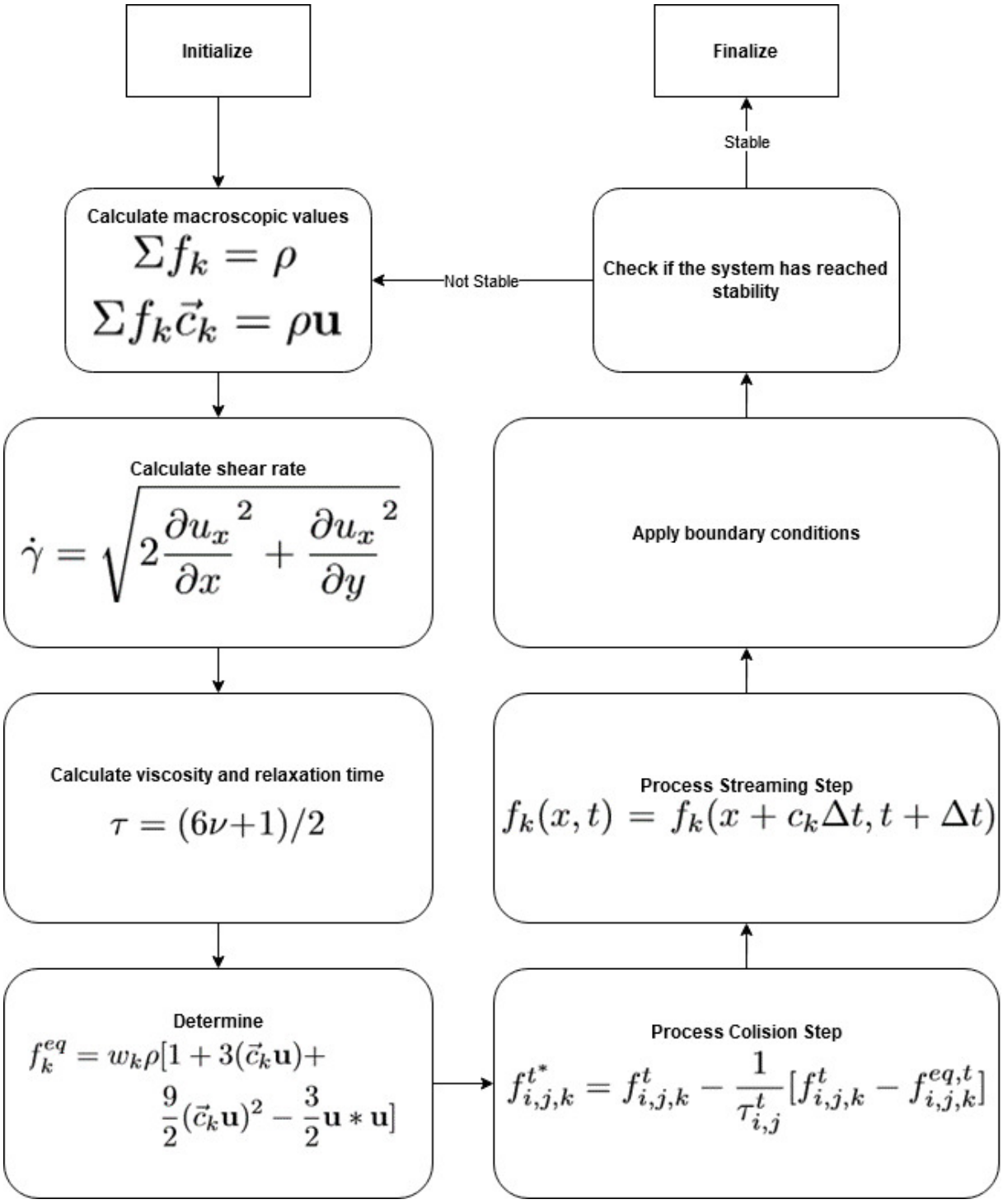

Figure 8: Flowchart showing the process of modelling a Non-Newtonian flow profile

3.3 Determining the electrical conductivity profile

In section 2.1 a relation between electrical conductivity and shear rate is described. This means that with the model from section 3.2, a electrical conductivity profile at any point in the flow cell can be determined, provided that a relation between electrical conductivity and shear rate exists for the fluid modelled. Figure 9 shows a relation between the shear rate and electrical conductivity of the fluid modelled in this paper.

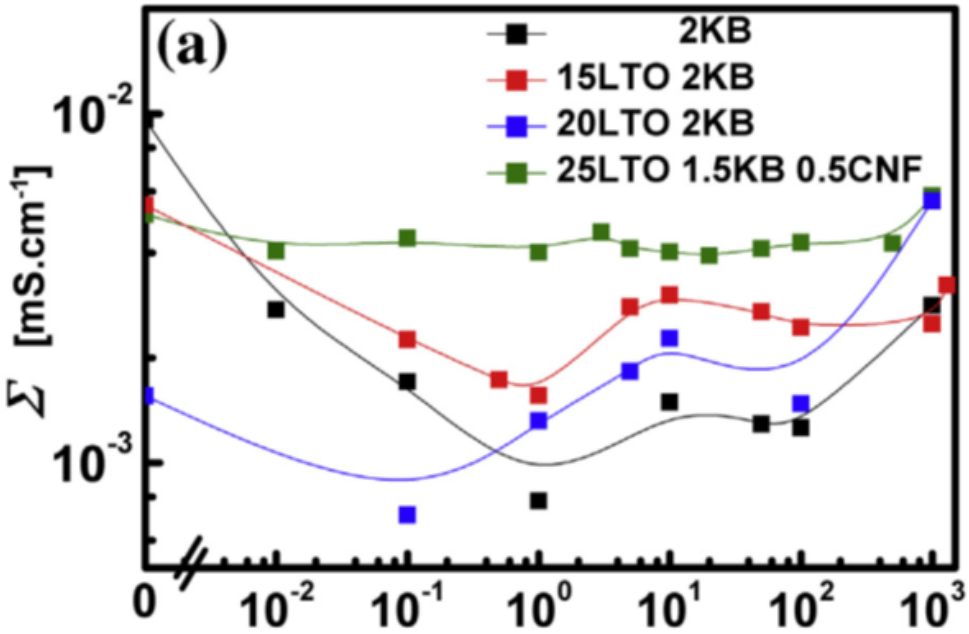

Figure 9: Data correlating the electrical conductivity Σ to the shear rate γ [5].

The data for the suspension 20LTO2KB from figure 9 is extrapolated using WebPlotDigitizer [14]. From the relation between the shear rate and electrical conductivity, electrical conductivity profiles within the flow cell can be created.

Knowing the electrical conductivity at all points in the flow cell means that the electronic resistance of the path of an electron can be determined. electrical conductivity and electronic resistance relate to one another via equation 37. [16]

$$R = \frac{L}{A\sigma(y)} \tag{37}$$

In this equation A is the size of the current collector in the flow cell. Equation 37 can be rewritten to equation 38 if the assumption is made that an electron travels straight from the bottom of the flow cell to the top. This is not physically correct, but does provide insight into how the electronic resistance changes over the length of the flow cell.

$$R_y = \frac{1}{A}\int_0^y \frac{1}{\sigma(y)} dy' \tag{38}$$

Since in the model the electrical conductivity is a discrete, not continuous, function of y (or x), the integral in equation 38 has to be rewritten. In order to rewrite the integral, the left Riemann sum will be used, which result in the following equation.

$$R_y = \frac{1}{A}\Delta x \Sigma_0^{n-1} \frac{1}{\sigma(a + n * \Delta y)} \tag{39}$$

Here $\Delta x = \frac{b-a}{n}$, where b is the y-coordinate of the top wall of the flow cell, a is the y-coordinate of the bottom wall of the flow cell, and n is the amount of values for the electrical conductivity, which is equal to $widthsize = 40$. With equation 39 it can be shown how the electronic resistance of the suspension in the flow cell changes over the length of the flow cell, assuming that the electron travels in a straight line from the bottom of the flow cell wall to the top of the flow cell wall.

4 Results

4.1 Poiseuille Flow

In order to check whether the modelled flow is accurate, several things have to be checked. First it must be checked that the modelled system has reached a stable state. Then it must be established that the flow profile properly develops from the initial conditions set. This means that from the set initial conditions the flow must continuously change until it reaches the state of a developed flow, meaning that sudden, or unexpected changes in the flow profile developement have to be explained. Finally the most developed profile in the simulation can be compared to the analytical solution for a developed flow, as these should be similar.

4.1.1 Stability of the flow profile

In order to check how stable the flow profile is, the density in the middle of the inlet is measured. Since the velocity at this point is determined in the initial conditions, the density is the only macroscopic property that can vary. The inlet of the system needs feedback from the outlet of the system in order to become properly stable.

The inlet of the system needs feedback from the outlet of the system in order to become properly stable. From the boundary conditions set at the inlet of the flow cell, a wave propagates to the outlet, where the wave is set to match the boundary conditions at the outlet. The arrival of the wave at the outlet increases the values for f_2, f_3 and f_4, and the boundary condition at the outlet then decreases the values for f_6, f_7 and f_8 in order to maintain a constant ρ. The particle distributions f_6, f_7 and f_8 then travel back to the inlet, where they effect the particle distributions f_2, f_3 and f_4. This process repeats, where particle distributions changed at one side of the flow cell travel to the other, causing changes in the particle distributions there. Because of this the density at the center of the flow cell is expected to behave like a harmonic oscillator.

In addition, this means that the system requires a minimum amount of time steps equal to twice the flow cell length, since this is the minimal amount of time steps it takes for the inlet to receive feedback. The development of density over time can be seen in figure 10.

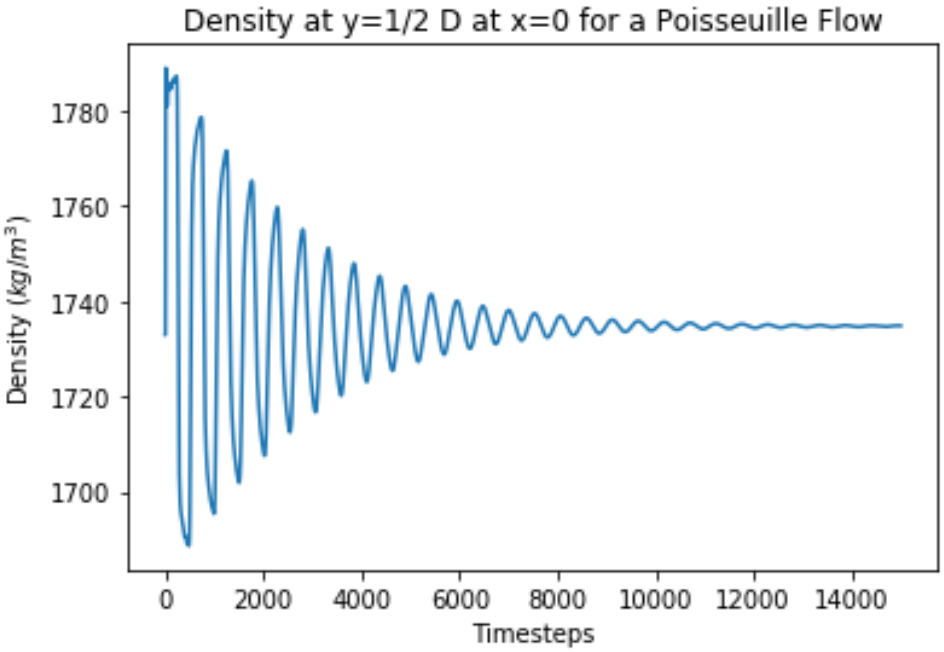

Figure 10: The development of the density in the inlet $x = 0$ at $y = \frac{1}{2}D$

From figure 10 it becomes apparent that the system reaches a fully stable state at $t = 15.000$.

4.1.2 Development of the flow profile

Now the development of the flow profile over the length of the flow cell will be checked. In figure 11, it can be seen how the flow profile develops.

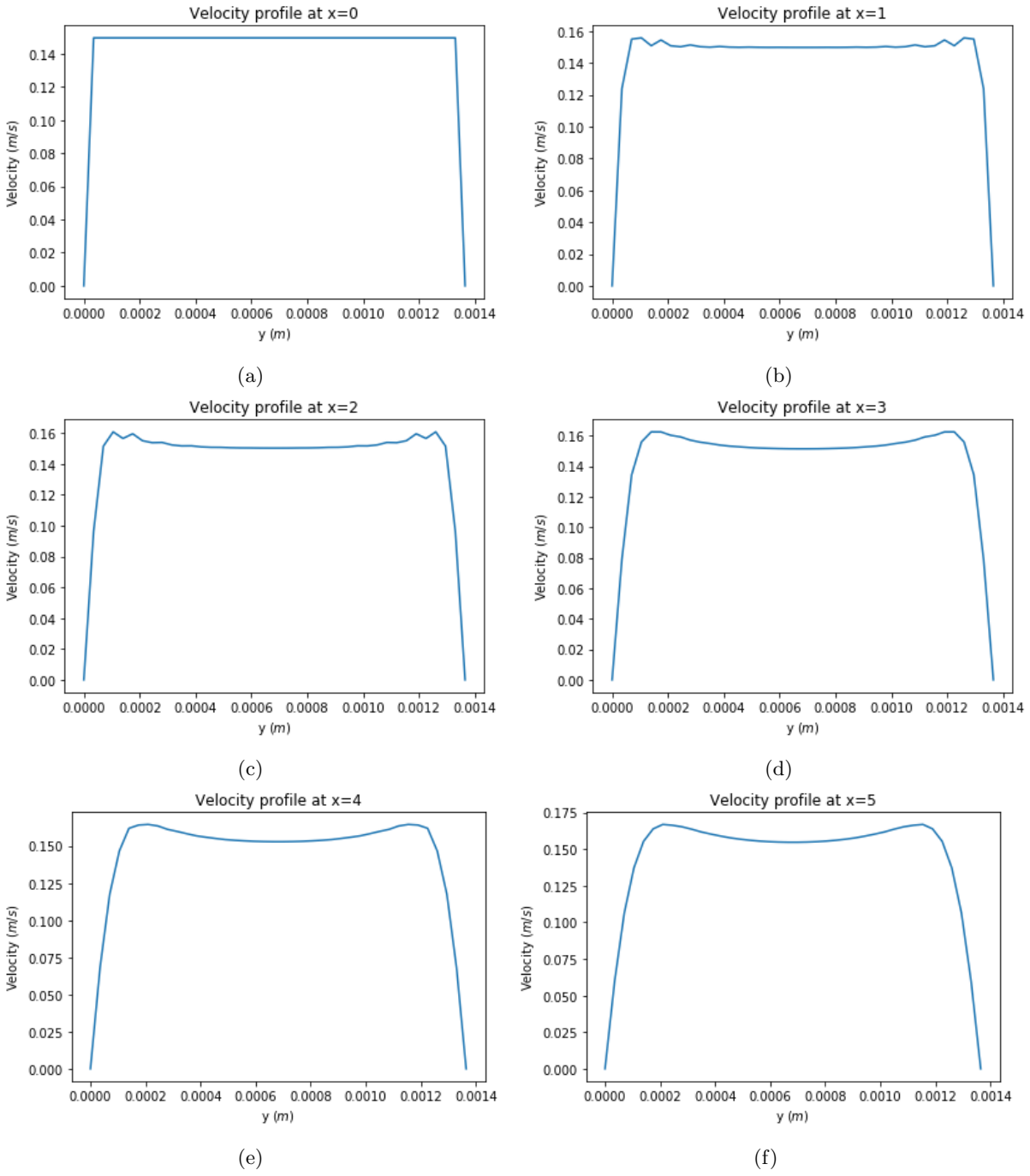

(a) (b) (c) (d) (e) (f)

Figure 11: Flow profiles from $x = 0$ to $x = 5$. In these graphs x is defined in Lattice Boltzmann units.

The initial conditions are still properly met after the flow is modelled, namely the velocity is equal to $u_{initial} = 0.15ms^{-1}$ everywhere except at the boundaries at $x = 0$, as can be seen in figure 11a. Then the zero-velocity at the boundaries starts affecting the flow, meaning that points closer to the wall decrease in speed. This process can be seen in figures 11b, 11c, 11d, 11e and 11f.

In figure 12 the further development of the flow can be seen.

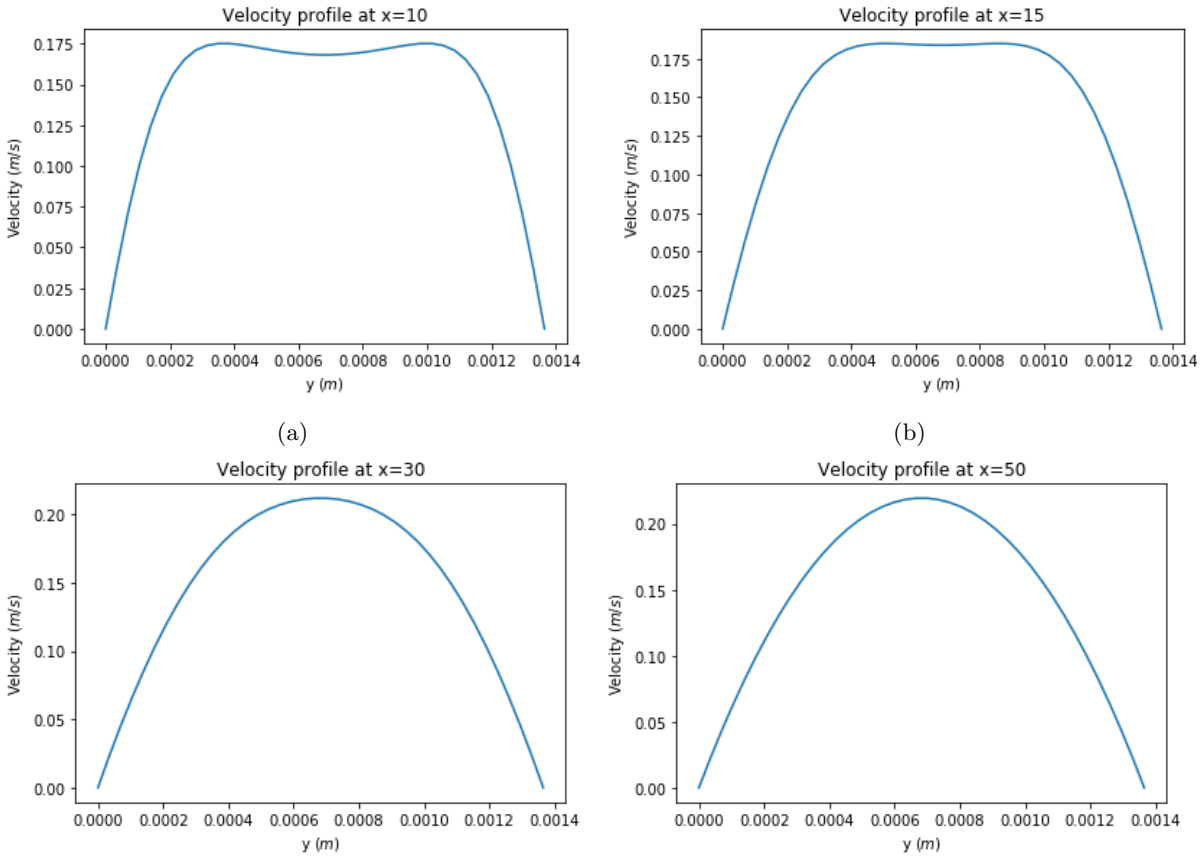

(a) (b)

(c) (d)

Figure 12: Flow profiles from $x = 10$ to $x = 50$. In these graphs x is defined in Lattice Boltzmann units.

The flow still develops significantly between $x = 10$ and $x = 15$, as can be seen in figures 12a and 12b. Between $x = 30$ and $x = 50$ the profile does not develop much anymore, but the change is still significant. In the flow profile produced by the model an irregularity can be spotted in figures 11b, 11c, 11d, 11e and 12a. The velocity is lower in the center of the flow cell than it is closer to the sides of the flow cell, which is not physically correct behavior, as the suspension experiences more resistance closer to the walls of the flow cell. A possible reason for this error could be that a boundary is not correctly applied, but the error will be discussed in more detail in section 5.

In order to demonstrate the possible compressibility error described in section 2.3.2, a density profile at $x = 10$ has been plotted in figure 13, where it can be seen that the absolute difference is less than 0.01% of the density.

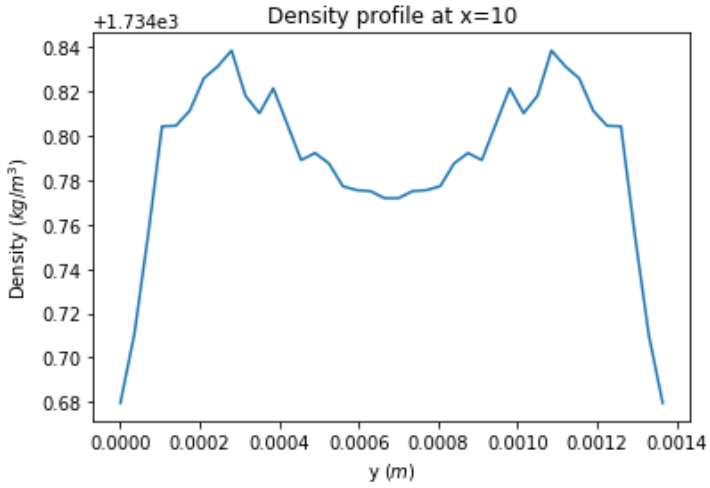

Figure 13: Density profile at $x = 10$. Maximum difference is $0.16kg/m^3$, an error of $1.0e-2\%$

In order to compare the final flow profile to the analytical solution, first the analytical solution has to be defined. The analytical solution of a Poisseuille flow in a channel of width D is defined as [8]:

$$u_x = u_0 * (1 - \frac{(y - \frac{1}{2}D)^2}{\frac{1}{4}D^2}) \tag{40}$$

Here u_0 is defined as the maximum speed in the final flow profile. This analytical solution for a Poisseuille flow is then compared to the final flow profile in the model in figure 14.

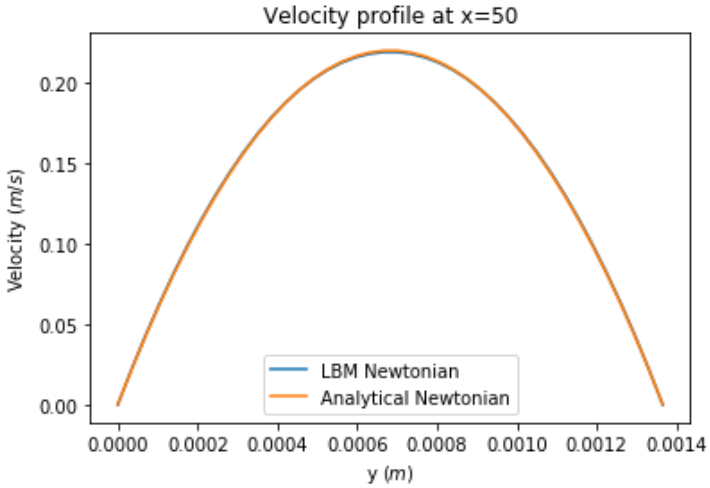

Figure 14: The most developed flow profile compared to the analytical solution of a Poisseuille flow.

In figure 14 the modelled flow and the analytical solution coincide perfectly, meaning that the model creates an accurate representation of a Poisseuille flow. This means that the code can now be altered to model a flow profile of a non-Newtonian fluid, such as the suspension of the Semi-Solid Flow Battery. The model does produce erroneous results for small x, so it will be considered inaccurate for small x.

4.2 Modeling a non-Newtonian flow

In order to model the flow profile for a non-Newtonian fluid, only a single parameter is altered, namely the relaxation time τ. The implementation of the code described in section 3.2 should result in a developed flow that is less parabolic than what can be seen in section 4.1.
The change in flow profile is a result of the dependence of the apparent viscosity on the shear rate.

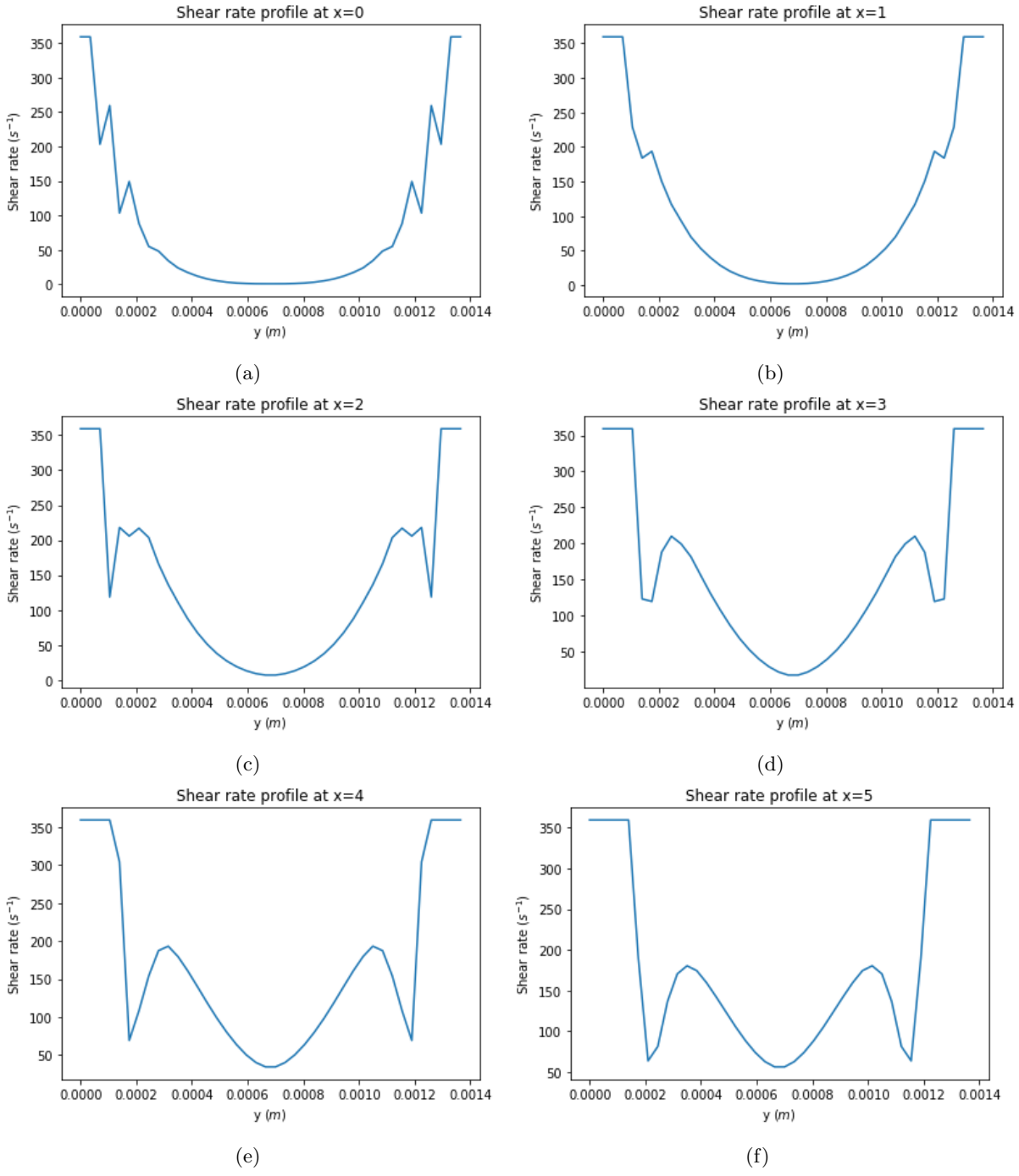

Figure 15: Shear rate profiles profiles from $x = 0$ to $x = 5$. In these graphs x is defined in Lattice Boltzmann units.

As can be seen the shear rate at the edges is locked at $\dot{\gamma} \approx 350$, because this is the highest defined shear rate in figure 7. It must be noted that a shear rate profile has a more complex shape than a velocity profile, since the shear rate depends on the velocity of surrounding lattice points and its own, whereas the velocity only depends on the particle distributions f_k at a singular lattice point. The shear rate further develops, as can be seen in figure 16

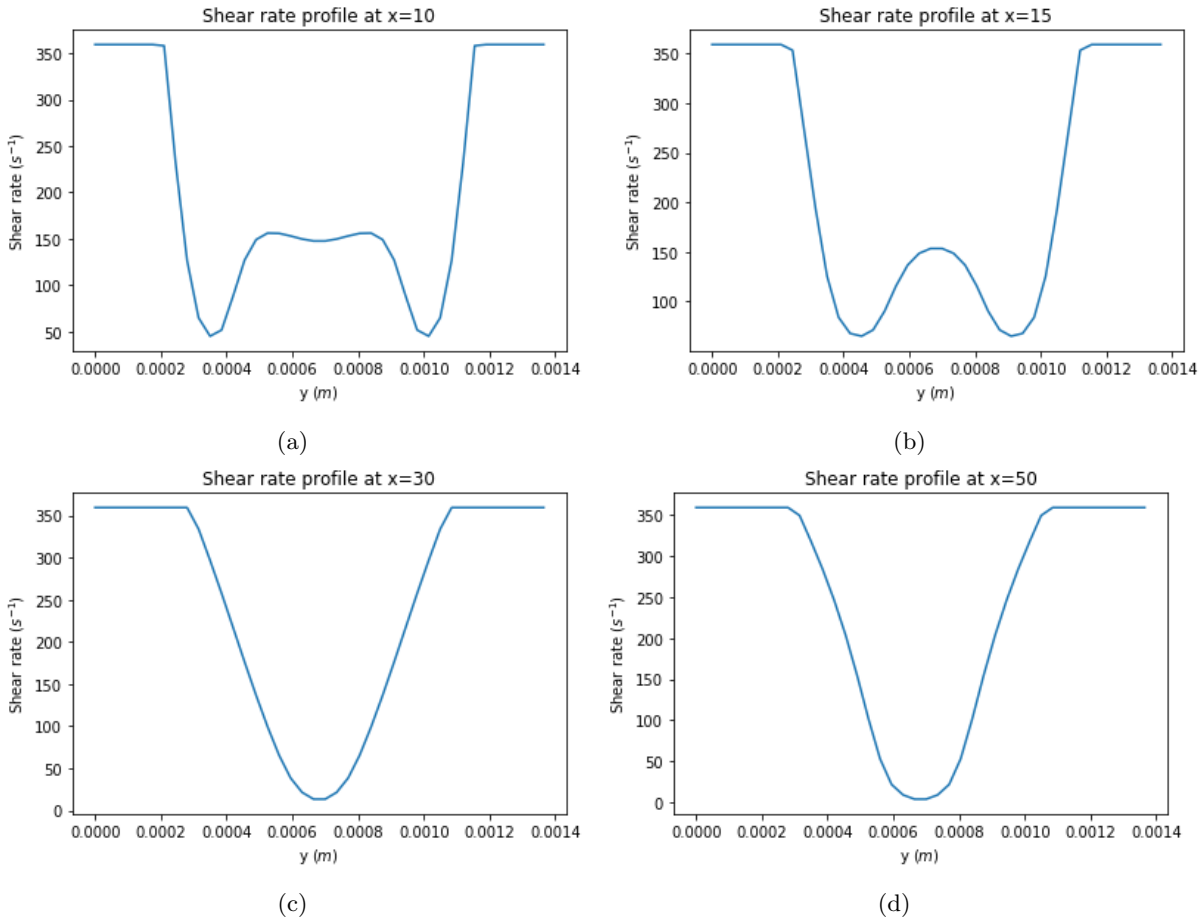

Figure 16: Shear rate profiles profiles from $x = 0$ to $x = 5$. In these graphs x is defined in Lattice Boltzmann units.

These shear rates result in a different viscosity, and these viscosity profiles have been plotted. The shear rate profiles from figure 15 and figure 16 lead to the viscosity profiles in figure 17.

These viscosity profiles are extrapolated from the data shown in section 3.2. The development of the flow profile greatly changes due to the change in viscosity, as can be seen in figure 18.

The velocity profile of the non-Newtonian fluid develops similarly to that of a Newtonian fluid as can be seen in figures 11 and 12. A big difference to be noted is the flat top of the flow profile as can be seen in figures 18g and 18h, which is consistent with the theoretical expectation of how a developed shear thinning velocity profile behaves. In figure 19 the analytical solution for a Newtonian velocity profile is compared to the velocity profile from figure 18h, here the flattening of the velocity profile can clearly be seen.

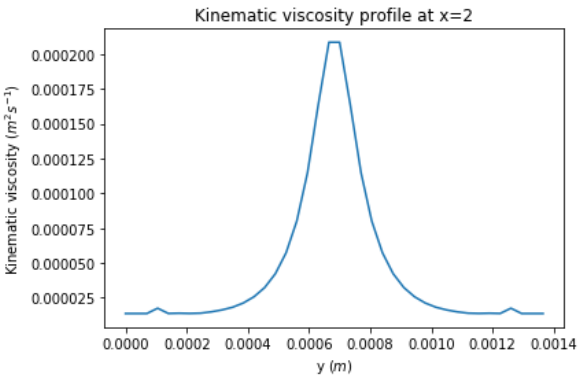

(a)

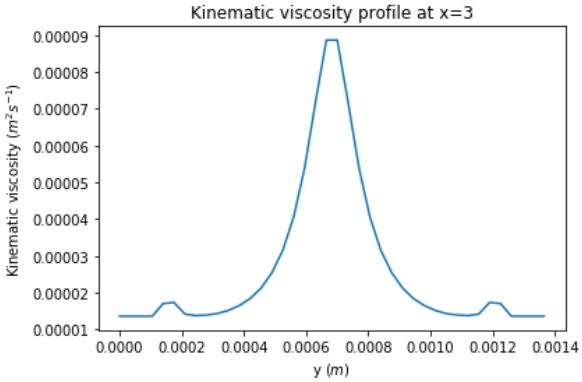

(b)

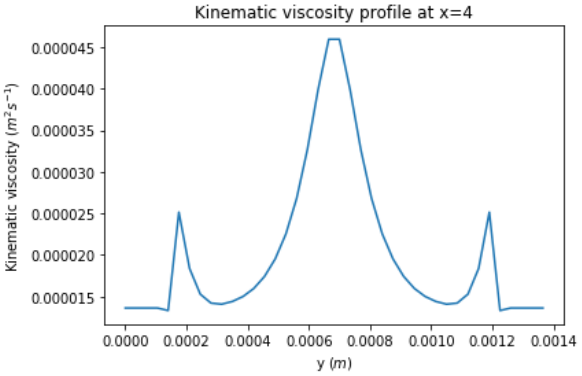

(c)

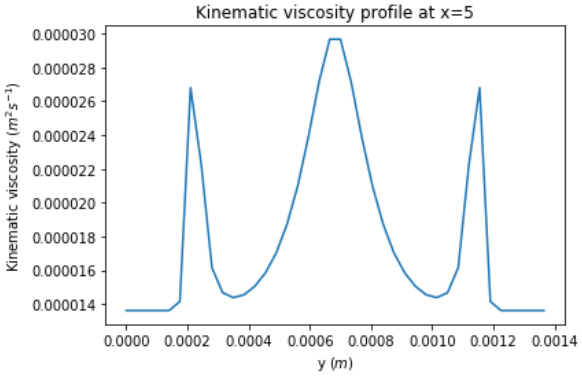

(d)

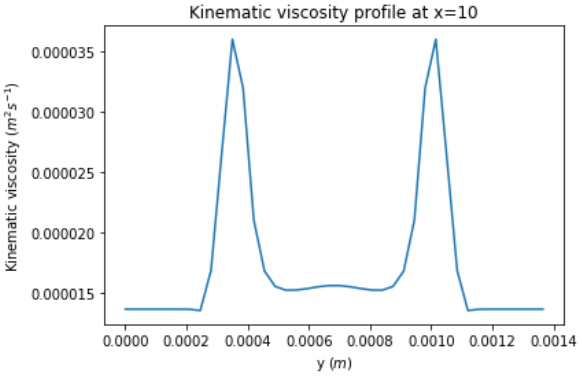

(e)

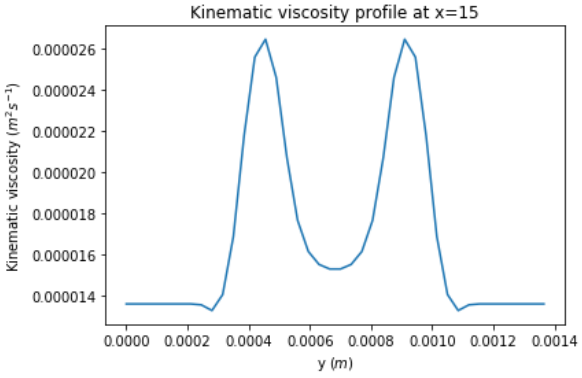

(f)

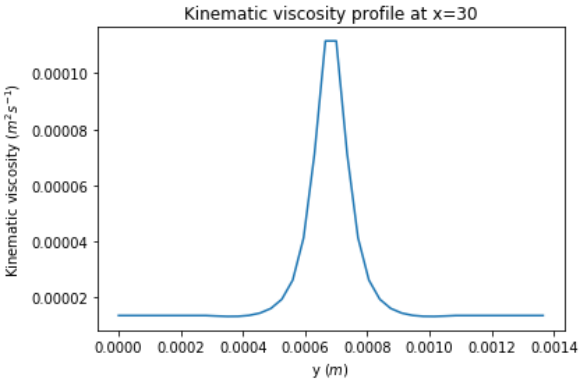

(g)

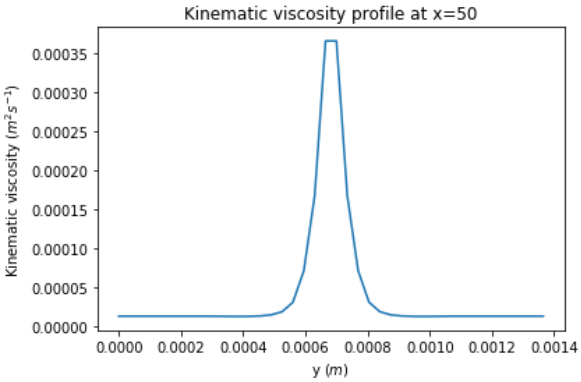

(h)

Figure 17: Kinematic viscosity profiles from $x = 2$ to $x = 50$.

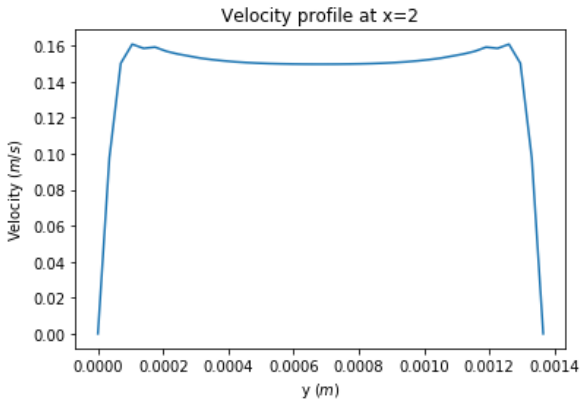

(a)

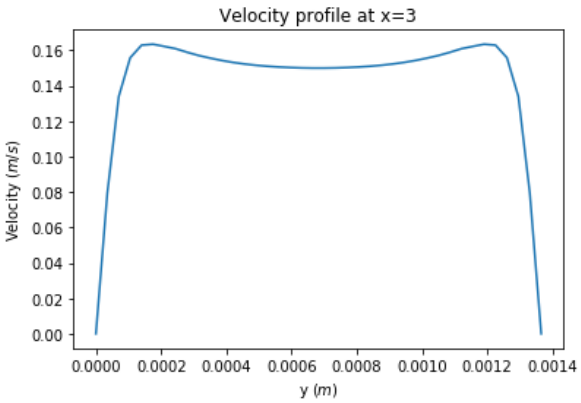

(b)

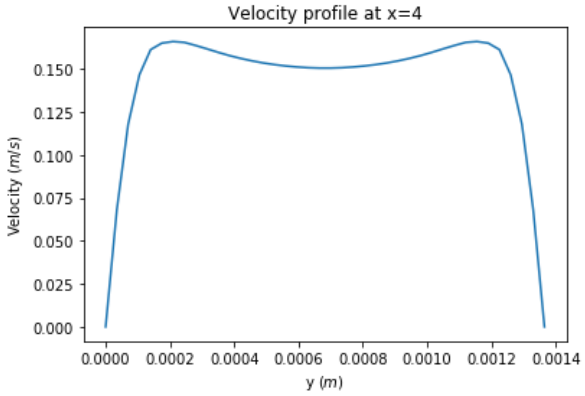

(c)

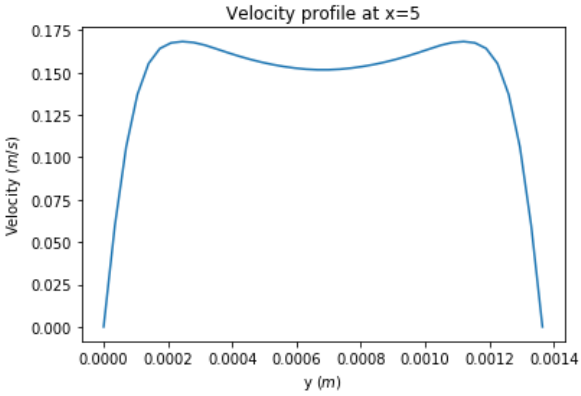

(d)

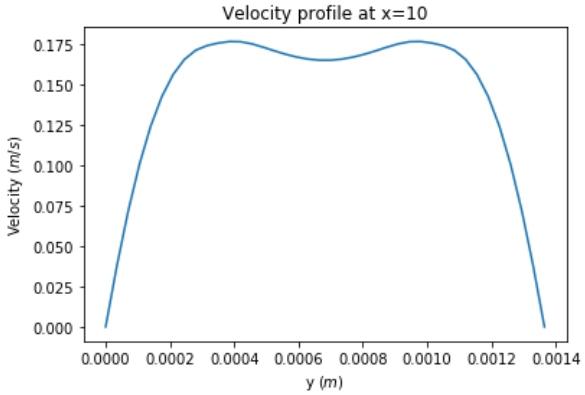

(e)

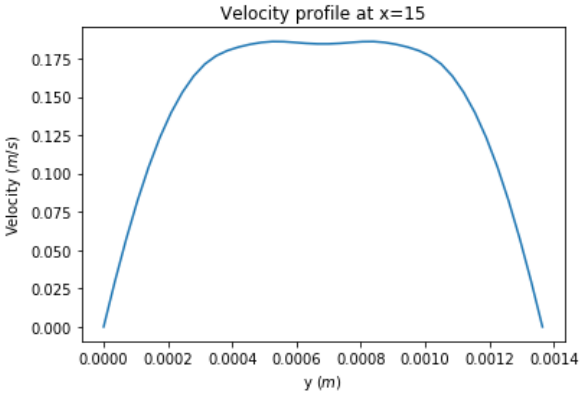

(f)

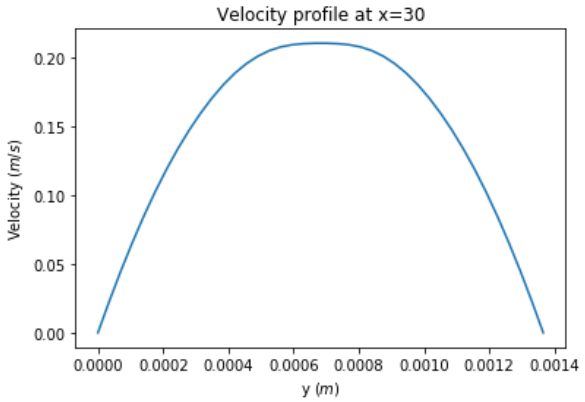

(g)

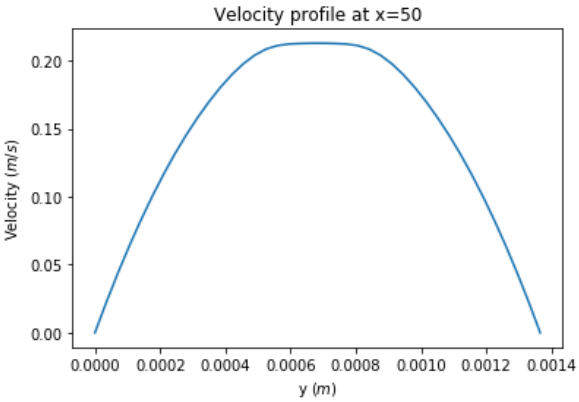

(h)

Figure 18: Velocity profiles from $x = 2$ to $x = 50$.

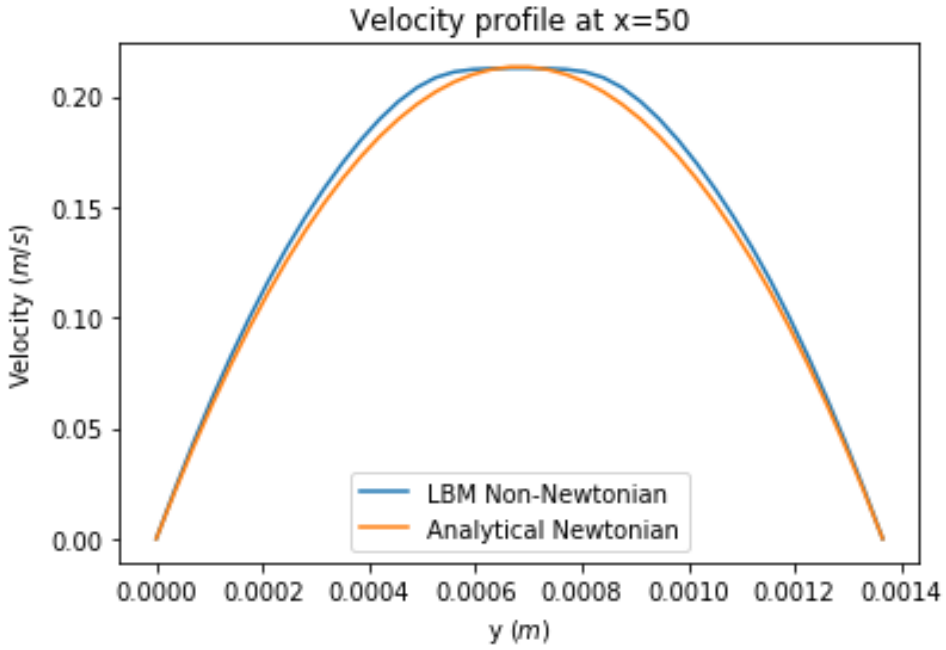

Figure 19: A comparison between the analytical velocity profile of a Newtonian fluid compare to the modeled velocity profile of a non-Newtonian fluid

4.3 Determining the electrical conductivity profile

With the shear rate profiles from section 4.2 and the coding described in section 3.3, electrical conductivity profiles for the developing flow profile can be set-up. Like the flow profile within the flow cell, these electrical conductivity profiles change greatly over x, as can be seen in figure 20.
The change in the electrical conductivity profile is significant, all the way to $x = 50$. Electrical conductivity profiles can be used to determine the electronic resistance via equation 38 in section 3.3, so the change in electronic resistance over the flow cell can be plotted. Figure 21 gives an approximation of how the electronic resistance of the fluid changes over the length of the flow cell.

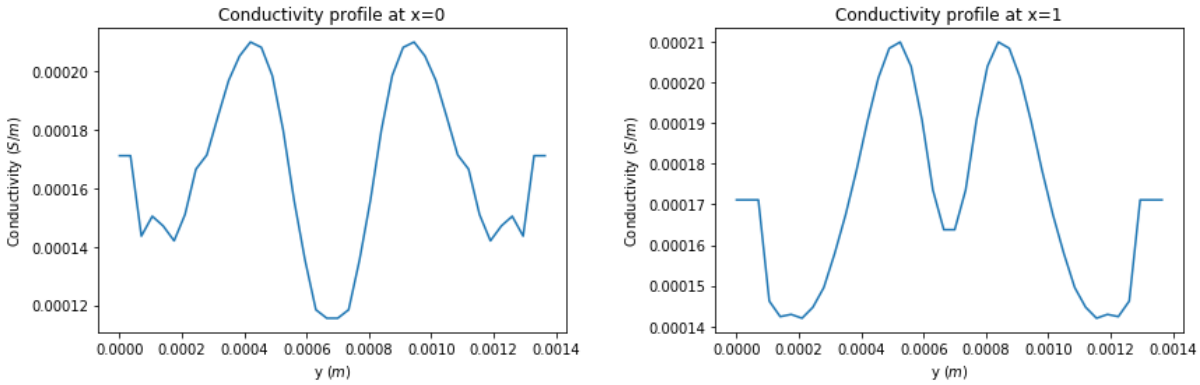

(a)

(b)

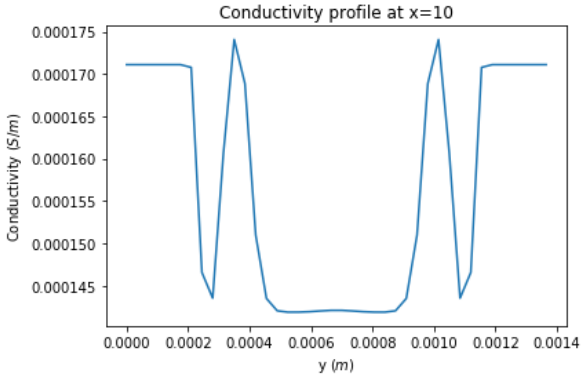

(c)

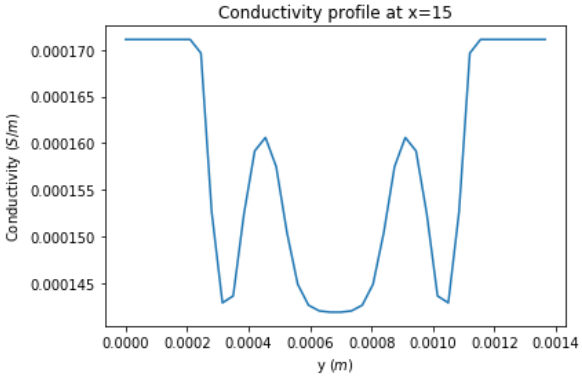

(d)

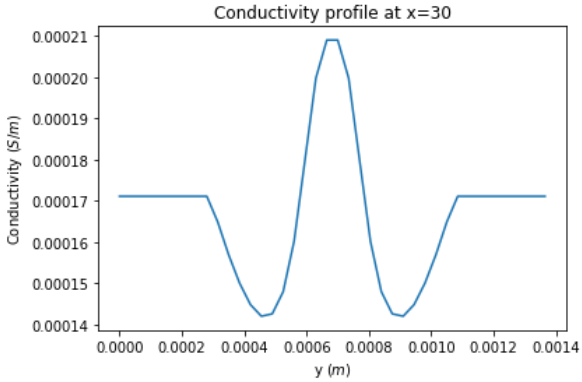

(e)

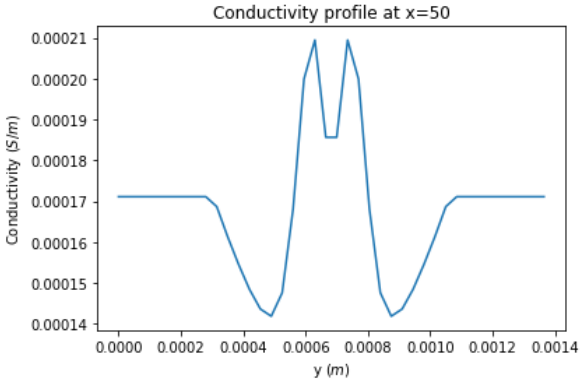

(f)

Figure 20: Electrical conductivity profiles from $x = 2$ to $x = 50$.

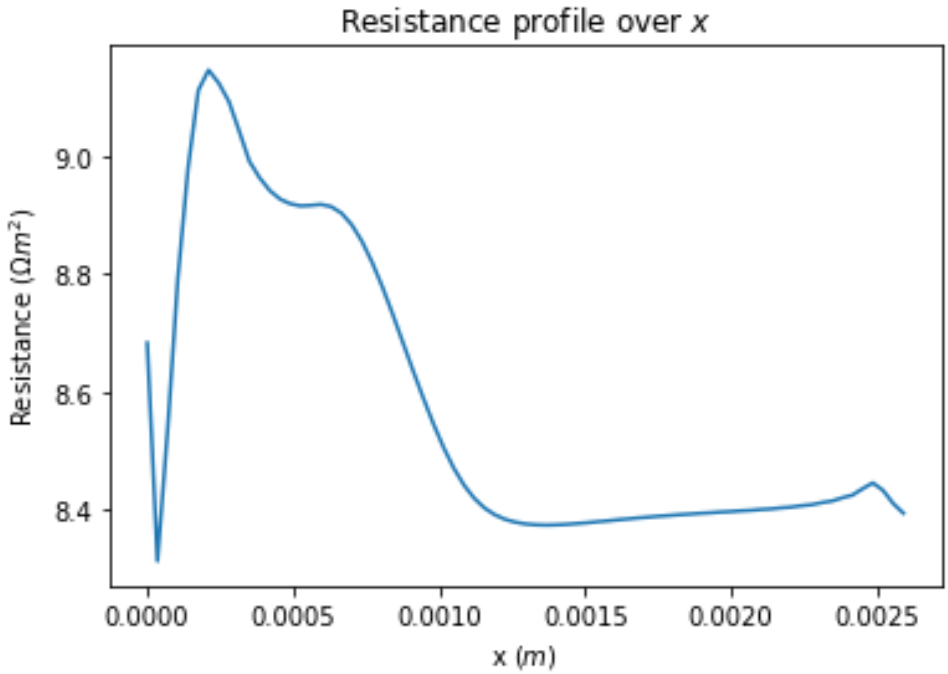

Figure 21: Electronic resistance of the suspension over the length of the flow cell

5 Discussion

5.1 Development of the flow

At the end of section 2.3.2, the compressibility error of the Lattice Boltzmann Method is mentioned. The maximum compressibility error is 0.54%. The compressibility error is therefore considered to be negligible.

The flow within the flow cell develops rapidly, as it fully develops over the distance of a few millimeters. The velocity at the center of the flow cell increases, as the velocity near the sides of the flow cell decreases as the flow develops. For the Poiseuille flow, the flow profile develops to the expected analytical expected flow, whereas the non-Newtonian flow profile differs from the analytical Poiseuille flow, due to the effect of the shear rate.

The most import error within the report to discuss is the dip visible in figures 18a, 18b, 18c, 18d and 18e, or similar velocity profiles for the Poiseuille flow. This error propagates inwards from the edges of the flow cell, and is almost gone at $x = 15$, though the error completely vanishes at $x = 20$. From this we can deduce that the error is caused by a boundary condition at the corner nodes at $x = 0$ not being applied properly. More specifically, since the error propagates into the flow cell diagonally, it is known that within the code f_4 at the top corner node and f_2 at the bottom corner node are determined erroneously. Since the error is symmetrical, it seems to cancel itself out after $x = 20$, leading to accurate flow profiles beyond that point, as can be seen in figures 18g and 18h. This means that the build model is considered inaccurate for any value $x \leq 20$.

The shear rate at the walls is greatest due to the velocity drop that occurs here, and decreases near the center, where the effect of the flow cell walls cannot be felt anymore. The flat shape of the developed non-Newtonian fluid $20LTO2KB$, is caused by the change in viscosity due to the change in shear rate. This flat profile is expected of a shear thinning fluid, and is comparable to the developed velocity profile determined by Rinus Smit [16].

5.2 Shear rate and electrical conductivity profiles

While modelling the non-Newtonian fluid, 20LTO2KB, several things have to be taken into account. First, the sharp edges visible in figures 15a and 15c. These sharp edges are caused by the width of the model being relatively small. Increasing the width of the model would remove the sharp edges, but would also greatly increase computation time. The capping visible in figure 17 at the walls of the flow cell needs to be addressed. The capping is not caused by an error in the code, but is implemented on purpose. Because the shear rates measured are far larger than the shear rates for which the viscosity and electrical conductivity are known. Therefore shear rates larger than $350(s^{-1})$ are shown to be equal to $350(s^{-1})$. At shear rates higher than this maximum value, the viscosity and electrical conductivity are considered to be constant, meaning that the capping of the shear rate does not affect the accuracy of the model. It can also be noted that the shear rate approaches, but never reaches 0, which is also because for shear rates lower than $10^{-2}(s^{-1})$ viscosity and electrical conductivity are considered constant.

The electrical conductivity profiles from section 4.3 show sharp edges akin to those seen in shear rate profiles. This is caused by the small width, in Lattice Boltzmann units, of the model. The capping in the electrical conductivity profiles happens for the same reason it does in the shear rates profiles in figure 17. Since a maximum and minimum shear rate are defined, capping of electrical conductivity is observed at the corresponding values. The electronic resistance profile that is derived from the electrical conductivity profiles shows interesting behavior of the electronic resistance over the flow cell. At any point for $x \leq 20lbu$ has to be considered inaccurate due to the error in the velocity profiles before this point. Additionally it has to be taken into account that profiles describe the electronic resistance if an electron travels from the bottom wall of the flow cell to the top wall of the flow cell at a given x in a straight line. This does not accurately describe the motion of an electron within the Semi-Solid Flow Battery, and only serves to show how the change in electrical conductivity throughout the flow cell affects the electronic resistance. It can be seen that the electronic resistance is path dependent and dependant on the starting and end point of the electron.

6 Conclusion

The research question this report aimed to answer was how the flow profile within the Semi-Solid Flow Battery developed, and how this development possibly affected the electrical conductivity and electronic resistance of the suspension.

In the model of the flow cell the flow development was modelled of the first $2.5mm$. Within this small distance the flow develops to the point where it is indistinguishable from a fully developed analytical flow. This means that after $2.5mm$ the flow can be considered to be fully developed. The development of the flow profiles creates varying shear rate profiles. The process used to model both the Poiseuille flow and the non-Newtonian suspension yielded inaccurate results in the first $0.7mm$ of the flow cell, hence any results from that area of the flow cell are considered inaccurate.

The shear rates found when modelling the non-Newtonian fluid $20LTO2KB$ were used to determine electrical conductivity profiles throughout the flow cell. These electrical conductivity profiles change rapidly, as even the smallest change in shear rate alters the electrical conductivity of the suspension. The electrical conductivity is then used the calculate the electronic resistance, under the assumption that electrons travel in a straight line from the bottom to the top of the flow cell. Though nothing can be said of the electronic resistance at the start of the flow cell, the electronic resistance constantly changes along the length of the flow cell. The continuous changes in electronic resistance show that there are electron paths that experience significantly less electronic resistance than others. This means that dependent on the path of the electron the efficiency of the Semi-Solid Flow battery changes.

From the results of the modelling it can be concluded that only at the very beginning of the Semi-Solid Flow Battery the development of the flow affects the electronic resistance. Only in the first few millimeters of the flow cell do the flow profiles change significantly, after which they can be considered fully developed. This means that in practice, if the flow cell of the SSFB were to be directly connected to the storage tank of the suspension, the electronic resistance would only vary at the very beginning of the flow cell. As long as there is a slight distance between the storage tank and flow cell of the SSFB, the development of the flow within the battery has a negligible effect on the efficiency of the Semi-Solid Flow battery.

7 Recommendations

With the model described in this report a variety of things about the semi-solid flow battery can researched. First, with the developing flow profile for a non-Newtonian fluid from section 4.2, it can be determined how much power is needed to force the suspension through the flow cell. This along with the electronic resistance profile from section 4.3 allows for an optimal set-up of the Semi-Solid Flow Battery to be determined. An optimal set-up would be one where both the power needed to pump the suspension through the battery and the electronic resistance of the suspension are low, provided that a low electronic resistance leads to a higher voltage produced by the battery. The set-up of the SSFB refers to the initial flow velocity, chosen suspension and the dimensions of the flow cell. In order to determine what an optimal set-up would be, the exact relation between electronic resistance and voltage produced by the SSFB would have to be determined. Since a relation between the set-up of the battery and the electronic resistance was determined within this report, a relation between the set-up of the SSFB and the voltage produced by the SSFB can be found.

The electrical conductivity profiles from section 4.3 can be used to properly determine the electronic resistance that an electron experiences when travelling through the flow cell. In order to determine the electronic resistance, first the path electrons travel has to be properly determined, since within this report the electronic resistance is only considered over a straight line. Research has already been done into this subject by Hugo Korthals Atles [17], and this research could be combined with the model from this paper in order to make definitive statements about the electronic resistance of the SSFB. This research can be done for all forms of carbon additive, as long as a relationship between shear rate and electrical conductivity is known for the additive in the substance.

References

[1] Sid Megahed, Bruno Scrosati, Lithium-ion rechargeable batteries, Journal of Power Sources, Volume 51, Issues 1–2, 1994, Pages 79-104, ISSN 0378-7753, https://doi.org/10.1016/0378-7753(94)01956-8.

[2] Gi, Z., Koening, G.M. (2017). Review Article: Flow battery systems with solid electroactivematerials. Journal of Vacuum Science and Technology B 35, 040801 https://doi.org/10.1116/1.4983210

[3] A description of varying non-newtonian rheologies [online] Available at:

`https://www.rheosense.com/applications/viscosity/newtonian-non-newtonian` [Accessed 13 Nov. 2020]

[4] Youssry, M., Madec, L., Soudan, P., Cerbelaud, M., Guyomard, D., Lestriez, B., (2013). Non-aqueouscarbon black suspensions for lithium-based redox flow batteries: rheology and simultaneous rheo-electrical behavior.Phys Chem Chem Phys. 2013;15(34):14476-14486. doi:10.1039/c3cp51371h

[5] Youssry, M., Madec, L., Soudan, P., Cerbelaud, M., Guyomard, D., Lestriez, B., (2014). Formulationof flowable anolyte for redox flow batteries for redox flow batteries: Rheo-electrical study.Journal ofPower Sources, vol. 274, pp.424-432, 2015.

[6] Duduta, M., Ho, B., Wood, V.C., Limthongkul, P., Brunini, V.E., Carter, W.C., Chiang, Y.M.,(2011). Semi-Solid Lithium Rechargeable Flow Battery.Adv. Energy Mater. 2011, XX, pp.1–6 https://doi.org/10.1002/aenm.201100152

[7] Weber, A.Z., Mench, M.M., Meyers, J.P. et al. (2011). Redox flow batteries: a review. J Appl Elec-trochem 41, 1137. https://doi.org/10.1007/s10800-011-0348-2

[8] Zou, Q., He, X., On pressure and velocity boundary conditions for the lattice Boltzmann BGK model. Physics of Fluids 9, 1591 (1997), https://doi.org/10.1063/1.869307

[9] Zou, Q., Hou, S., Chen, S., Doolen, G.D, An Improved Incompressible Lattice Boltzmann Model for Time-Independent Flows. J Stat Phys 81, 35–48 (1995). https://doi.org/10.1007/BF02179966

[10] Alankar, A., Prakash, A., (2016), Proc. of Fourth International Conference On Advances in Civil, Structural and Mechanical Engineering - ACSM 2016 ISBN: 978-1-63248-096-5 doi: 10.15224/ 978-1-63248-096-5-11

[11] Gabbanelli, S., Drazer, G., & Koplik, J. (2005). Lattice Boltzmann method for non-Newtonian (power-law) fluids. Phys. Rev. E, 72, 046312. doi: 10.1103/PhysRevE.72.046312

[12] Yamaguchi H. (2008) Non-Newtonian Fluid and Flow. In: Engineering Fluid Mechanics pp 399-496. Fluid Mechanics and Its Applications, vol 85. Springer, Dordrecht. https://doi.org/10.1007/978-1-4020-6742-6_7

[13] Rhode, M., (2004), Extending the lattice-Boltzmann method: Novel techniques for local grid refinement and boundary conditions, http://resolver.tudelft.nl/uuid:775b0255-84b6-4866-9ff2-921237969b7c ISBN: 90-6464-113-7

[14] Rohatgi, A., (2019). WebPlotDigitizer. Version 4.2.https://automeris.io/WebPlotDigitizer, San Fran-sisco, California, USA.

[15] Hoogstraten, H.W., (1985)., Collegedictaat Toegepaste Wiskunde II (Numerieke Methode).

[16] Smit, R., (2020). https://d1rkab7tlqy5f1.cloudfront.net/TNW/Afdelingen/Radiation Science and Technology/Research Groups/RPNM/Publications/BEP_Rinus_Smit.pdf

[17] Korthals Altes, H. (2020) https://d1rkab7tlqy5f1.cloudfront.net/TNW/Afdelingen/Radiation Science and Technology/Research Groups/RPNM/Publications/BEP_Hugo_Korthals_Altes.pdf